IEEE TRANSACTIONS ON

ENERGY CONVERSION

A PUBLICATION OF THE IEEE POWER ENGINEERING SOCIETY

MARCH 2005 VOLUME 20 NUMBER 1 ITCNE4 (ISSN 0885-8969)

(Contents Continued on Back Cover)

IEEE

(Contents Continued from Front Cover)

Development of a Thermofluid Model for Axial Field Permanent-Magnet Machines

Rong-Jie Wang, *Member, IEEE*, Maarten J. Kamper, *Member, IEEE*, and Robert T. Dobson

***Abstract*—In this paper, a thermofluid model combining a lumped parameter heat transfer model and an air-flow model of a typical axial-field permanent-magnet (AFPM) machine is developed. The accuracy and consistency of the derived model are assessed by comparing the calculated flow rate and temperature values of a prototype machine with the measured ones. The developed thermofluid model is shown to perform thermal calculations with reasonable accuracy.**

***Index Terms*—Air cooling, axial field, heat transfer, permanent-magnet machine, thermal modeling.**

NOMENCLATURE

A	Cross-section area of a flow path (m^2).
C_{mo}	Moment coefficient.
c_p	Specific heat at constant pressure (Joules per kilogram per Kelvin).
D	Diameter (in meters)
D_h	Hydraulic diameter (in meters).
D_o	Outer diameter of electric machine (in meters).
F	Friction force (in Newtons).
G	Gap ratio s/r_o.
Gr	Grashof number.
h	Local heat-transfer coefficient ($\mathrm{W/m^2\ K}$).
I_{ph}	Phase current of the machine (in amperes).
i	Enthalpy (in Joules per kilogram).
k	Thermal conductivity (in watts per meter per Kelvin).
k_i	Loss coefficient.
k_s	Slip factor.
M_o	Momentum ($\mathrm{N \cdot s}$).
$\dot{m}$	Mass flow rate (in kilograms per second)
n	Machine rotation speed (r/min).
n_b	Number of blades.
Nu	Nusselt number.
P, p	Power (in watts), pressure (in pascals).
P_r	Prandtl number.
$\wp$	Wetted perimeter (in meters).
$\dot{Q}$	Heat-transfer rate into a system (in watts).
Q	Volumetric flow rate ($\mathrm{m^3/s}$).
R	Thermal resistance (in Kelvin per watt).
R, r, r_o	Radius, outer radius (in meters).
Ra	Rayleigh number.
Re	Reynolds number.
s	Axial gap between rotor and stator (in meters).
T	Temperature (°C or Kelvin).
U	Internal energy (in Joules per kilogram).
u_1, u_2	Inlet, outlet tangential velocity (in meters per second).
v_1, v_2	Inlet, outlet absolute velocity (in meters per second).
$\dot{W}$	Rate of doing work (in watts).
w_1, w_2	Inlet, outlet radial velocity (in meters per second).

Greek Symbols

ρ	Density ($\mathrm{kg/m^3}$).
β	Coefficient of thermal expansion ($\mathrm{K^{-1}}$).
ϵ	Emissivity.
σ	Stefan–Boltzmann constant ($\mathrm{W/m^2\ K^4}$).
ω	Angular velocity (rad/s).
μ	Dynamic viscosity (in kilograms per meter per second).
ν	Kinematic viscosity ($\mathrm{m^2/s}$).
λ	Friction factor.
λ_T	Turbulent parameter.
γ	Equivalent sand grain roughness (in meters).
Δ	Finite difference.

Subscripts

a	Surrounding air.
ag	Air gap.
amb	Ambient.
c, $conv$	Convection.
cs	Control surface.
Cu	Copper.
cv	Control volume.
$cond$ or d	Conduction.
d	Developed.
e	Environment, exit.
edy	Eddy current.
f	Friction.
h	Hydraulic.
i	In, inlet, input.
l	Energy losses.
m	Magnet.
mo	Moment.

Manuscript received April 29, 2003; revised June 17, 2003. This work was supported by the University of Stellenbosch and SA industry. Paper no. TEC-00107-2003.

R.-J. Wang and M. J. Kamper are with the Department of Electrical Engineering, University of Stellenbosch, Matieland 7602, South Africa (e-mail: kamper@sun.ac.za).

R. T. Dobson is with the Department of Mechanical Engineering, University of Stellenbosch, Matieland 7602, South Africa.

Digital Object Identifier 10.1109/TEC.2004.837301

out	Output.
p	Periphery.
r	Radiation, rotor.
T	Turbulent.
t	Total.
wf	Windage and friction.

I. Introduction

THE advent of new high-energy product permanent-magnet (PM) materials has opened up great opportunities for novel topologies of electrical machines with advantageous features such as high efficiency and power/weight ratio. An axial flux permanent magnet (AFPM) machine, with an axially directed magnetic field crossing the air gap, has a remarkably short axial length and can find applications in power generation, light traction drives, electric pump, and fan drives. Fig. 1 shows the layout and active components of a typical AFPM machine.

Whereas extensive research has been devoted to thermal studies of conventional electrical machines, AFPM machines have received very little attention [1]. Since AFPM machines possess relatively large air-gap volume and quite often have multiairgaps, the general perception is that AFPM machines have better ventilation capacity than their radial field counterparts [2], [3].

However, like conventional machines, AFPM machines are also subject to cooling problems. To ensure a long operational life for the machine, the heat generated must be removed from the machine so that the temperature limitations established for the machine materials such as insulating materials, lubricants, and PMs are complied with. Besides, lower operating temperature reduces extra copper losses introduced by the temperature coefficient of the winding resistance. Thus, quantitative studies of the heat dissipation potential of AFPM machines with vastly different topologies are clearly needed.

This paper presents a thermofluid model of an AFPM machine. First, the fluid flow model of a typical AFPM machine is developed, where the relationships between flow rate and rotating speed are obtained. With this information available, a lumped-parameter heat transfer model of the AFPM generator is then derived and used to estimate the operating temperatures in various parts of the machine for different power-generating conditions. Experimental tests are also done on the prototype machine and results are compared with the calculated ones.

II. Fluid-Flow Model

Close examination of the machine structure shown in Fig. 1 reveals that an air stream will be drawn through the air inlet holes into the machine and then forced outwards into the radial channel as the rotor discs rotate. The PMs act as impeller blades. The fluid behavior of the AFPM machine is much like that of a centrifugal fan.

A. Ideal Radial Channel

According to the theory of an ideal impeller, the following assumptions have to be made to establish the one-dimensional (1-D) flow model of the ideal radial channel [4], [5].

a) Inlet flow to the channel is radial.

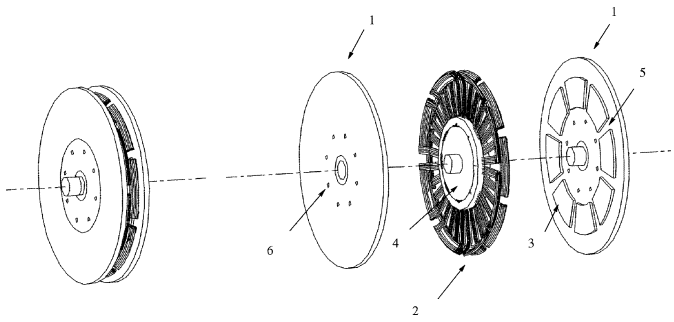

Fig. 1. Exploded view of an AFPM machine, 1: rotor discs, 2: stator winding, 3: permanent magnets, 4: epoxy core, 5: radial channels, and 6: air-inlet holes.

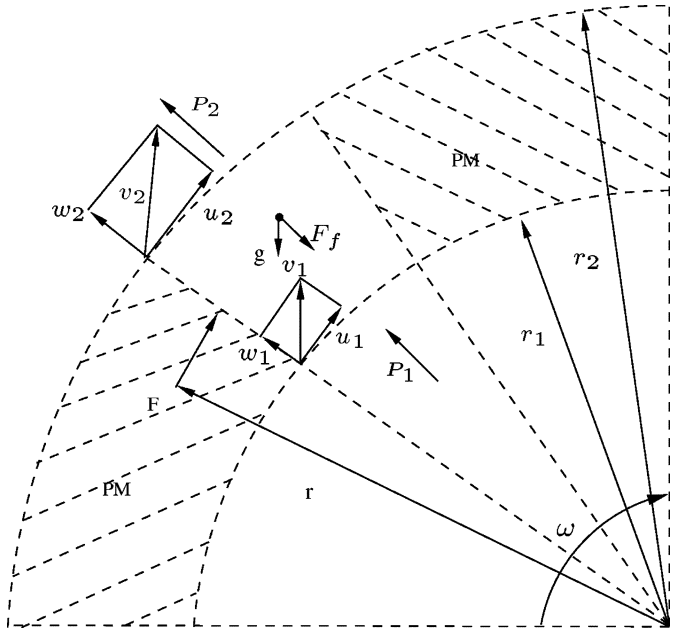

Fig. 2. Velocity triangles for a PM channel.

b) No tangential flow component in the radial channels.

c) Flow is incompressible and frictionless.

d) Velocity variation across the width or depth of the channel is zero.

Fig. 2 shows a radial channel with the velocity triangles drawn at the inlet and the outlet. It can be observed that the pressure at the inlet p_1 and the outlet p_2 and the friction F_f make no contribution to the sum of the momentum $\sum M_0$. If gravity is ignored, the general representation of conservation of momentum takes the form [6]

$$\sum M_0 = \frac{\partial}{\partial t}\left[\int_{cv}(\vec{r}\times\vec{u})\rho dV\right] + \int_{cs}(\vec{r}\times\vec{u})\rho(\vec{w}\cdot\vec{n})dA. \quad (1)$$

For steady-state 1-D air flowing between the entrance and exit of the channel, (1) is simplified as

$$\sum M_0 = T_0 = (\vec{r_2}\times\vec{u_2})\dot{m}_2 - (\vec{r_1}\times\vec{u_1})\dot{m}_1 \quad (2)$$

where $\dot{m}_2 = \dot{m}_1 = \rho Q$, and $u = \omega r$. The input shaft power $\dot{W}_i$ is then given by

$$\dot{W}_i = T_0 \cdot \omega = \rho Q \omega^2 (r_2^2 - r_1^2). \quad (3)$$

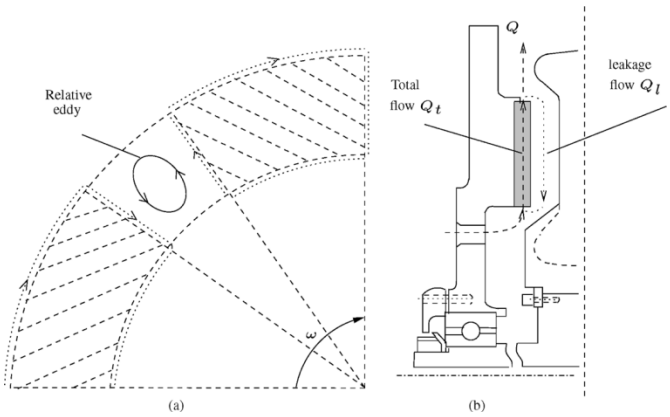

Fig. 3. Slip and leakage in an AFPM machine, where (a) there is relative eddy in the PM channel. (b) Leakage flow in an AFPM machine (not to scale).

Rearranging the above equation gives

$$\frac{\dot{W}_i}{Q} = \rho\omega^2(r_2^2 - r_1^2). \tag{4}$$

Based on the principle of conservation of energy, the input shaft power may be given as

$$\dot{W}_i = \dot{m}\left(\frac{p_2 - p_1}{\rho} + \frac{w_2^2 - w_1^2}{2} + z_2 - z_1 + U_2 - U_1\right). \tag{5}$$

If potential $(z_2 - z_1)$ and the internal energy (friction) are ignored, (5) may be written in the same units as (4) as

$$\frac{\dot{W}_i}{Q} = (p_2 - p_1) + \rho\frac{w_2^2 - w_1^2}{2}. \tag{6}$$

If (4) and (6) are equated and noting that $w_1 = Q/A_1$ and $w_2 = Q/A_2$ (A_1 and A_2 are cross-sectional areas of the inlet and outlet channel, respectively), the pressure difference Δp between the entrance and exit of the radial channel (shown in Fig. 2) may be expressed as

$$\Delta p = p_2 - p_1 = \rho\omega^2\left(r_2^2 - r_1^2\right) - \frac{\rho}{2}\left(\frac{1}{A_2^2} - \frac{1}{A_1^2}\right)Q^2. \tag{7}$$

Equation (7) may be termed the *ideal* equation describing the air flow through the radial channel.

B. Actual Radial Channel

The actual characteristics of a hydraulic machine differ from the ideal case due to two reasons: the uneven spatial distribution of velocities in the blade passages and the leakage and recirculation of flow together with hydraulic losses such as friction and shock losses. These are completely different issues [4] and shall be dealt with separately in the following two sections as *slip* and *shock, leakage, and friction*.

1) Slip: As a result of the unbalanced velocity distribution on the leading and trailing edges of a PM channel and rotation effects [5], there exists, due to Stodola, a relative eddy [5], [7] within the blade passage shown in Fig. 3(a). This results in the reduction of the tangential velocity components and is called slip, which is usually accounted for using a slip factor. For purely radial blades, the Stanitz slip factor k_s ($80° < \beta_2 < 90°$) is

$$k_s = \frac{1–0.63\pi}{nb}. \tag{8}$$

When applying a slip factor, the pressure relations (7) become

$$\Delta p = \rho\omega^2(k_s r_2^2 - r_1^2) + \frac{\rho}{2}\left(\frac{1}{A_1^2} - \frac{1}{A_2^2}\right)\cdot Q^2. \tag{9}$$

2) Shock, Leakage, and Friction: Energy losses due to friction, separation of the boundary layer (shock loss), and leakage should also be considered. As illustrated in Fig. 3(b), if the total volumetric flow rate through the PM channel is Q_t, the pressure difference between the PM exit and the entrance will cause a *leakage* or recirculation of a volume of fluid Q_l, thus reducing the flow rate at outlet to $Q = Q_t - Q_l$. The Q_l is a function of mass flow rate and discharge and leakage path resistances. The leakage flow reaches its maximum when the main outlet flow is shut.

These losses can be accounted for by introducing a pressure loss term Δp_l in (9) as follows [5]:

$$\Delta p = \rho\omega^2(k_s r_2^2 - r_1^2) + \frac{\rho}{2}\left(\frac{1}{A_1^2} - \frac{1}{A_2^2}\right)\cdot Q^2 - \Delta p_l. \tag{10}$$

3) System Losses: As the air passes through the AFPM machine, the system pressure loss due to friction must be accounted for. The sum of these losses is given by

$$\Delta p_f = \frac{\rho Q^2}{2}\sum_{i=1}^{n}\frac{k_i}{A_i^2}. \tag{11}$$

There are a number of sections through which the air flows in the AFPM machine (Fig. 4):

1) entry to the rotor air inlet holes;
2) passage through rotation short pipe;
3) bending of air from pipe to annulus (90°);
4) round-bend air passage (90°);
5) contraction of air in tapering passage;

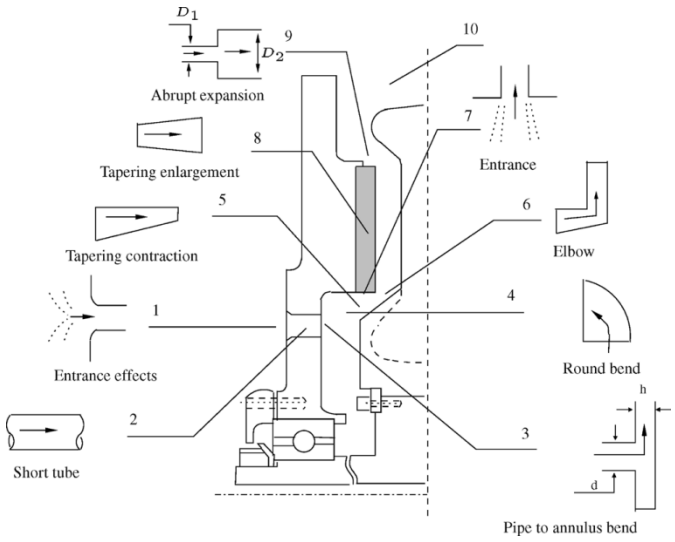

Fig. 4. System losses of an AFPM machine.

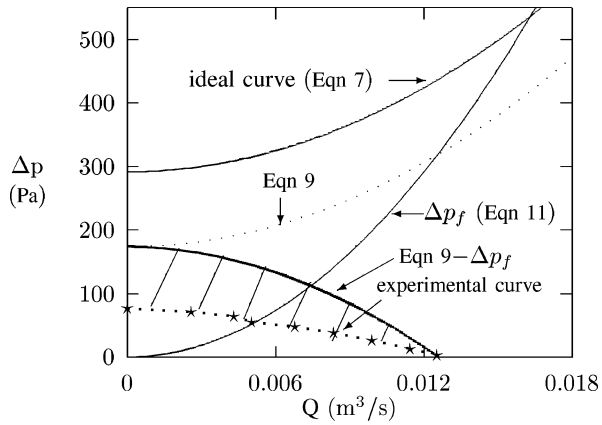

Fig. 5. Losses and characteristics curves at 1200 r/min.

6) bending of air through the 90° elbow;
7) entry to permanent-magnet (PM) channels;
8) expansion of air through tapering enlargement;
9) abrupt expansion of air on the exit of the channel;
10) expansion as the air leaves the opening of the parallel rotor discs.

The loss coefficients associated with each section are readily available in the literature [7]–[9]. Where the section is not circular, use has been made of hydraulic diameter to characterize the cross section. The hydraulic diameter is defined as $D_h = 4A/\wp$, where A is the cross-sectional area of the flow path, and $\wp$ is the wetted perimeter.

The loss coefficient for a pipe is given by $\lambda L/d$, where λ is a friction factor obtained as a function of Re and surface roughness from a Moody diagram [10]. To facilitate numeric calculations, the Moody diagram may be represented by [8]

$$\begin{cases} \lambda &= 8\left[\left(\frac{8}{Re}\right)^{12} + \frac{1}{(A+B)^{3/2}}\right]^{1/12} \\ A &= \left[2.457 \cdot ln\left\{\frac{1}{\left(\frac{7}{Re}\right)^{0.9} + \frac{0.27\gamma}{D}}\right\}\right]^{16} \\ B &= \left[\frac{37\,530}{Re}\right]^{16} \end{cases} \tag{12}$$

where $Re = \rho D_h Q/\mu A$.

4) Characteristics: It is now possible to relate the theoretical prediction obtained from the ideal flow model to the actual characteristic by accounting for the various losses discussed above. Since the AFPM machine (Fig. 1) has two identical coaxial rotating discs operating on the same stator, it may be treated as two identical fans in parallel. The characteristic curve presented in this section represents only half of the AFPM machine. The characteristic curve of the whole machine may be obtained by adding flow rate at the same pressure.

Assuming that the AFPM machine operates at a constant speed of 1200 r/min, the ideal developed pressure characteristic for a radial channel is a function described by (7), as shown in Fig. 5.

After introducing the slip factor, the resultant curve is shown by a dotted line as (9). It was not possible to obtain a suitable correlation in the literature [11] for the pressure loss due to shock and leakage as was the case for the slip. The calculated characteristic curve without considering shock and leakage losses [(9) $-\Delta p_f$] shown in Fig. 5 is significantly higher than the experimental one. The shaded area in Fig. 5 represents the shock and leakage losses. It can be seen that at low flow rates, the shock and leakage losses are greater but tend to zero at the maximum flow rate. The calculated maximum flow rate point corresponds with the experimental curve. Although it could be a coincidence, it may be assumed at this stage that the influence of shock and leakage losses at the maximum flow rate is insignificant.

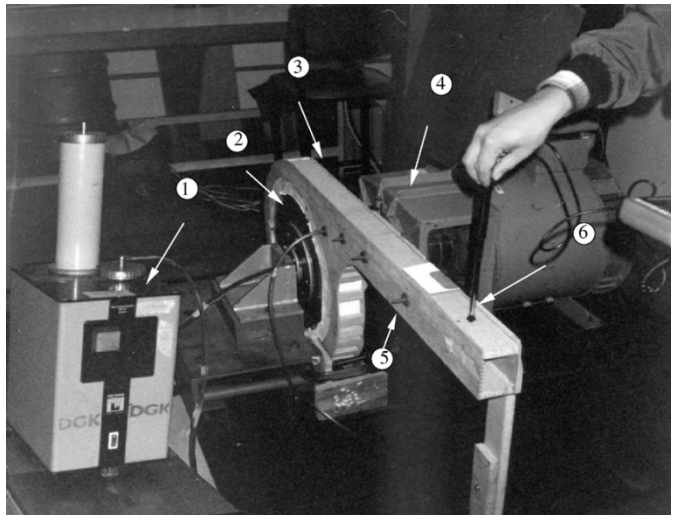

Fig. 6. Experimental setup, where 1: manometer, 2: AFPM machine, 3: discharge duct, 4: drive machine, 5: pressure tapping point, and 6: hot-wire anemometer probe.

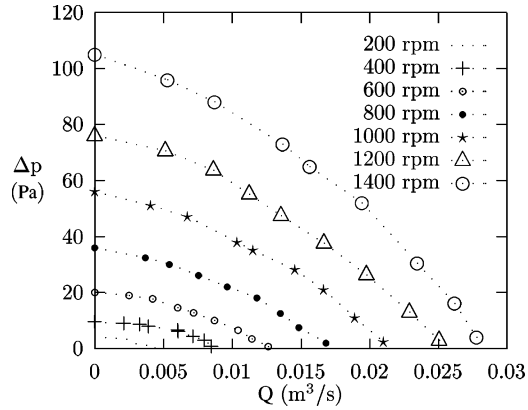

Fig. 7. Measured characteristic curves of pressure against flow rate for the AFPM machine ($\rho = 1.177$ kg/m^3).

5) Flow and Pressure Measurements: In order to check the validity of the fluid flow model, experimental tests were performed. The AFPM machine was driven by a dc motor (at no load) and allowed to operate as a conventional fan, as shown in Fig. 6. The machine was set up with a discharge duct. Along one side of the duct, several tapping points were made for measuring the static pressure with a manometer. Near the outlet of the duct, a provision was made whereby the velocity is measured using a hot-wire anemometer probe.

The static pressure difference Δp was measured as a function of volumetric flow rate $\dot{Q} = A \cdot v$ for different motor speeds varying from 200 to 1400 r/min. The results are plotted in Fig. 7. Note that the pressure losses occurring in the discharge duct have been subtracted from the measured values.

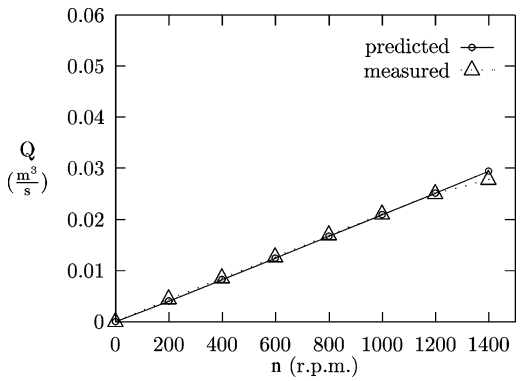

Fig. 8. Calculated and measured volumetric flow rate as a function of speed.

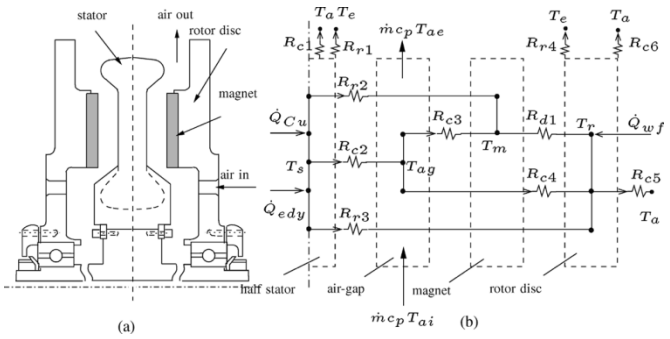

Fig. 9. Thermal resistance circuit of an AFPM generator.

6) Volumetric Flow Rate: Fig. 8 shows both the computed and measured volumetric flow rate of the AFPM machine (Fig. 1) at different operating speeds. Predicted results correlate well with the measured ones. This confirms that shock and leakage losses, as previously assumed, become less significant as the operating point is approached.

III. Thermal Model

Lumped-parameter circuits, consisting of a network of thermal resistances, nodal temperatures, and heat sources, have been widely used to represent the complex distributed thermal parameters of electrical machines [1], [12].

A. Thermal Resistance Circuit

Fig. 9(a) shows a sectional view of an AFPM machine. It can be observed that the AFPM stator is symmetrical from a heat transfer perspective. It is therefore reasonable to model only half of the machine [Fig. 9(b)].

The heat flowing through each path of the thermal resistance circuit is given by a temperature difference divided by a thermal resistance (Table I). The radiation resistance R_r may be easily derived as

$$R_r = \frac{\frac{1-\epsilon_1}{\epsilon_1 A_1} + \frac{1}{F_{12} A_1} + \frac{1-\epsilon_2}{\epsilon_2 A_2}}{\sigma (T_2 + T_1)(T_2^2 + T_1^2)}. \tag{13}$$

In this equation, it is seen that the radiation resistance depends on the absolute temperature, surface spectral property ϵ, and surface orientation taken into account by a form factor F.

TABLE I
Definition of the Thermal Resistances in Fig. 9(b)

Symbols	Definition
R_{c1}	Convection: stator end-winding to air
R_{c2}	Convection: stator to air-gap
R_{c3}	Convection: airgap to magnets
R_{c4}	Convection: airgap to rotor disc
R_{c5}	Convection: rotor disc to open air
R_{c6}	Convection: rotor periphery to air
R_{r1}	Radiation: end-winding to open air
R_{r2}	Radiation: stator to magnets
R_{r3}	Radiation: stator to rotor disc
R_{r4}	Radiation: rotor periphery to air
R_{d1}	Conduction: magnets to rotor disc

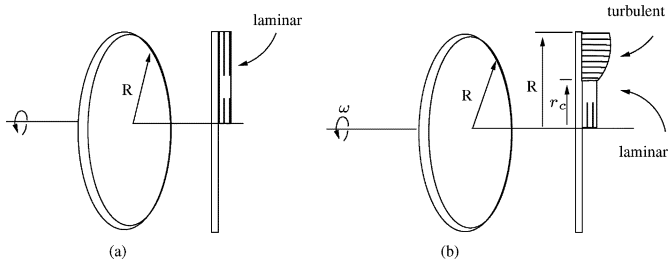

Fig. 10. Free rotating disc, with (a) laminar flow, (b) laminar and turbulent flow.

Convective heat transfer from a surface to a moving fluid depends on the heat-transfer coefficient, the determination of which is a complex problem, usually necessitating the use of empirically determined correlations. No convection heat-transfer correlations relating to the specific topology of AFPM machines are available, and for this reason, potentially suitable existing correlations are dealt with in the next section.

B. Convection Heat-Transfer Coefficients

The rotating disc system plays a major role in the cooling and ventilation of the AFPM machine. Accurately determining the convection heat-transfer coefficients needs thorough theoretical and experimental investigation because of the complexity of the flow regimes. In this section, the convection heat-transfer coefficients in different parts of the AFPM machine are evaluated, exploiting a number of existing models.

1) Free Rotating Disc: The average heat-transfer coefficient at the outside surface of a rotating disc may be evaluated using the formula developed for free rotating plate [14], that is

$$\bar{h} = \frac{k}{R} \cdot \overline{Nu} \tag{14}$$

where $\overline{Nu}$ is given according to different flow conditions as follows.

i) For combined effects of free convection and rotation in laminar flow [Fig. 10(a)] [14]

$$\overline{Nu} = \frac{2}{5} \cdot (Re^2 + Gr)^{1/4} \tag{15}$$

where $Re = \omega R^2/\nu$, $Gr = \beta g R^3 \pi^{3/2} \Delta T/\nu^2$, and ΔT is the temperature difference between the disc surface and the surrounding air.

ii) For a combination of laminar and turbulent flow with the transition at $r_c = (2.5 \times 10^5 \nu/\omega)^{1/2}$ [Fig. 10(b)] [14]

$$\overline{Nu} = 0.015 \cdot Re^{4/5} - 100 \cdot \left(\frac{r_c}{R}\right)^2. \tag{16}$$

It is instructive to compare the heat-transfer capabilities between a rotation disc and a stationary disc. Considering the AFPM machine depicted in Fig. 1, which has a diameter of 0.4 m and rotates at 1260 r/min, the convection heat-transfer coefficient may be calculated by using (14) and (16) as 41 W/m^2 K, which is about ten times that of the same disc at standstill. Alternatively, one can say that the effective heat dissipation area of the same disc can be increased by a factor of 10 when rotating.

2) Rotor Edge: The heat-transfer correlations for the radial periphery of the rotor disc are similar to those of a rotating cylinder in air. In this case, the average heat transfer coefficient is given as

$$\bar{h}_p = \left(\frac{k}{D}\right)\overline{Nu} \tag{17}$$

where $\overline{Nu} = 0.133 \cdot Re_D^{2/3} Pr^{1/3}$, D is the diameter of the disc, and $Re_D = \omega D^2/\nu$. When using (15)–(17), a uniform temperature distribution in the disc is normally assumed.

If these equations are applied to the rotor disc, the average heat-transfer coefficient around the radial periphery h_p can be computed, which is found to be about 95 W/m^{2}K and, therefore, justifies its presence in the thermal resistance circuit. Since h_p is proportional to the rotational speed ω, it may be concluded that the rotor periphery plays an increasingly important role in the heat dissipation as ω increases.

3) Rotor-Stator System: As seen in Fig. 1, the main heat-transfer region consists of surface-mounted PMs with radial channels between the PMs. Due to centrifugal effects, there is a forced flow through the PM channels, which increases the local heat-transfer rate compared to that of a free disc. The relative increase will depend on the gap ratio $G = s/r_o$, the mass flow rate, and the rotational speed of the system under consideration [15].

Having radial channels and thick impellers, an air-cooled AFPM machine may be regarded as a poorly designed fan from a fluid flow perspective. Its tangential velocity component is much larger than the radial component. Thus, the heat-transfer rate near the rotating disc shows more dependence on the rotational Reynolds number, which is defined as [16]

$$Re = \frac{\rho \omega^2 r_o}{\mu}. \tag{18}$$

Owen [17] provided an approximate solution for the flow between a rotating and a stationary disc, which relates the average Nusselt number to the moment coefficient of the stator-side rotor face C_{mo} by the following equation:

$$\begin{cases} \overline{Nu} = \frac{Re_r C_{mo}}{\pi} \\ C_{mo} Re_r^{1/5} = 0.333 \lambda_T \end{cases} \tag{19}$$

where λ_T is a turbulent parameter given as a function of volumetric flow rate Q as follows:

$$\lambda_T = \frac{Q}{\nu r_o} Re_r^{-4/5}. \tag{20}$$

With the average Nusselt number known, the average heat-transfer coefficient is obtained from (14). Applying the above approximate solution to the same AFPM machine operating at a speed of 1260 r/min with a measured radial flow of 0.026 m^3/s between rotor and stator, the estimated average heat-transfer coefficient from the stator across the air gap to the rotating disc is 94 W/m^{2}K.

As discussed in [16], it has been shown that for a small gap ratio ($G < 0.1$), the flow in the air-gap space between the rotor and stator can be treated as a boundary layer. While it is not necessarily true that the convective heat-transfer coefficient from the stator to the air flow is close to that from the air flow to the rotating disc, the same heat-transfer coefficient has been assumed in the thermal circuit simulation.

With all of the convection heat-transfer coefficients determined, the convection resistances shown in Fig. 9(b) are readily calculated by using $R_c = 1/hA$.

C. Conservation of Energy

If conservation of energy is applied, the rate of internal energy change of a control volume may be written as follows:

$$\frac{\Delta U}{\Delta t} = \dot{Q}_{\text{in}} - \dot{Q}_{\text{out}} + \dot{m}_{\text{in}} i_{\text{in}} - \dot{m}_{\text{out}} i_{\text{out}}. \tag{21}$$

For steady-state conditions, $\Delta U/\Delta t = 0$ and, therefore

$$0 = \dot{Q}_{\text{in}} - \dot{Q}_{\text{out}} + \dot{m}_{\text{in}} i_{\text{in}} - \dot{m}_{\text{out}} i_{\text{out}}. \tag{22}$$

Equation (22) is applied to each part (the half stator, air gap, magnet, and rotor disc) of the AFPM machine shown in Fig. 9 to obtain a set of equations with the temperatures of the parts being the only unknowns. The heat flowing in each path is given as a temperature difference divided by a thermal resistance. The values used for the heat source terms are given in [19], in which copper loss was calculated from measured rms phase current and phase resistance compensated by a temperature coefficient while the eddy current loss was obtained by using a novel method described in [20]. This set of equations is rather complex but is readily solved using, for example, the Gauss–Seidel iteration. Note that wherever mixed materials are present in the thermal model, new thermal properties are defined based on the proportion of different materials.

D. Temperature Measurements

The AFPM machine is driven by a dc motor as shown in Fig. 6 and operates as a generator feeding a rectifier load. Both rated and overload (double the rated current) operating conditions are monitored. The temperatures of the rotating disc and the peripheral edge of the windings are measured using a digital infrared thermometer.

The average winding temperature was measured using an electrical resistance method [12]. The machine was run for long enough to ensure steady-state conditions. The driving motor

TABLE II
PREDICTED AND MEASURED TEMPERATURE RISES ($T_{amb} = 23.75°C$, $I_{ph} = 30$ A, n = 1217 r/min)

Machine parts	Calculated (°C)	Measured (°C)
Stator winding	27.8	23.3
Rotor disc	14.1	11.2
Rare-earth PM	13.7	-
End-winding	-	21.5
Air-gap	7.6	-

TABLE III
PREDICTED AND MEASURED TEMPERATURE RISES ($T_{amb} = 24°C$, $I_{ph} = 60$ A, n = 1263 r/min)

Machine parts	Calculated (°C)	Measured (°C)
Stator winding	102.1	95.1
Rotor disc	27.3	25.5
Rare-earth PM	27.6	-
End-winding	-	65.4
Air-gap	30.1	-

was then shut down, and when the machine came to standstill, the electrical resistances of the three phases of the windings were measured as a function of time. A suitable curve was fitted to these resistance measurements, and the resistance that the winding would have had when the machine was shut down was determined by extrapolating back in time.

For ensuring the validity of the measurements, the first resistance reading should be taken within 30 s after switching off the power to the driving motor. The average temperature rise in the stator winding is then obtained by using the following equation:

$$\Delta T = \frac{R_2 - R_1}{R_1}(K + T_1) + T_1 - T_0 \tag{23}$$

where K is a constant ($K = 235$ for copper winding, $K = 228$ for aluminum winding), T_0 is the ambient temperature, T_1 is the cold winding temperature, and R_1 and R_2 are the cold and hot winding resistances, respectively.

IV. COMPARISON OF RESULTS

The computed values of the temperature rise in the various parts of the AFPM machine are compared with the corresponding measurements in Tables II and III. The calculated results agree reasonably well with the tested results, considering the relatively simple thermal resistance network used to represent the AFPM machine.

V. APPLICATION

A thermofluid model for calculating thermal behavior of AFPM machines has been developed and experimentally validated. To further verify the developed models, relevant thermal tests were carried out on a 250-kW power AFPM generator. This generator is shown in Fig. 11 together with an inlet duct to measure the air-flow rate.

The generator was running at about 1400 r/min with an rms phase current of 243 A. Table IV gives both measured and predicted temperature values for this machine. Note that in this case, the measured flow rate was used in the calculation. It can

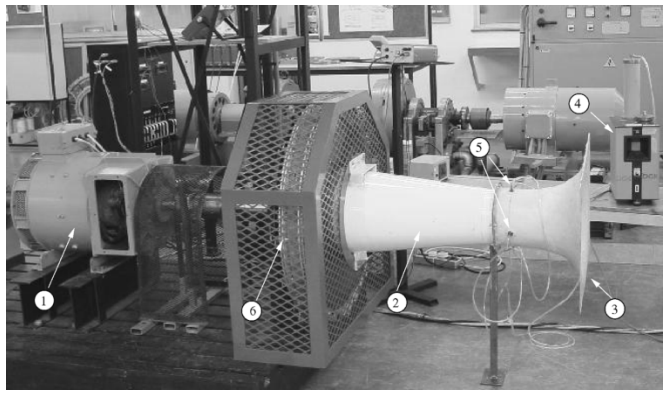

Fig. 11. Flow measurement of the prototype AFPM machine, where 1: dc machine drive, 2: inlet duct, 3: bell mouth, 4: manometer, 5: pressure tapping point, and 6: AFPM generator.

TABLE IV
MEASURED AND PREDICTED MACHINE TEMPERATURE RISES ($T_{amb} = 14.6°C$, $I_{ph} = 243$ A, n = 1402 r/min)

Machine part	Predicted ^oC	Measured ^oC
Stator winding	45.72	56.25
Air-gap	4.47	-
Rotor disk	5.46	3.9
Permanent Magnet	5.5	-

be seen that the measured stator temperature is higher than the predicted one. This may be caused by a) thermocouples that were all placed in the inner end winding of the stator winding where the temperature is at its highest, whereas the predicted values are the average temperatures of the stator; b) the measured flow rate is larger than the actual flow rate due to the effects of the inlet duct.

VI. DISCUSSION AND CONCLUSIONS

The main aim of this study is the development and verification of a thermofluid model for analyzing and predicting thermal behavior of AFPM machines. The comparison between the calculated and the measured results shows that the developed model can perform the thermal analysis with reasonable accuracy.

It should be noted that the determination of the air temperature in the air gap is only possible if the mass flow rate through the air gap can be somehow predicted, hence, the necessity of a reasonable fluid-flow model. The fluid-flow model gives reasonable results; however, it may be somewhat limited because the effect of rotation in the system losses as given in (11) was neglected.

The air flow through the AFPM machine is not optimized from a minimum energy loss point of view. By taking into account sound fluid mechanics practice, an improved mass flow rate could be achieved with a subsequent reduction in the operating temperature and, hence, a longer service life.

The developed fluid-flow model of the AFPM machine assumes an open-type enclosure where the air flow at the outer periphery is not obstructed. Based on the theory presented in this paper, it can be easily extended to represent the machine with the enclosed structure.

REFERENCES

[1] E. Spooner and B. J. Chalmers, "TORUS: A slotless, toroidal-stator, permanent-magnet generator," *Proc. Inst. Elect. Eng., B*, vol. 139, pp. 497–506, 1992.

[2] C. C. Chan, "Axial-field electrical machines with yokeless armature core," Ph.D. dissertation, Univ. Hong Kong, 1982.

[3] J. F. Gieras and M. Wing, *Permanent Magnet Motor Technology: Design and Applications*. New York: Marcel Dekker, 1997.

[4] J. F. Douglas, J. M. Gasiorek, and J. A. Swaffield, *Fluid Mechanics*. White Plains, NY: Longman, 1995.

[5] A. T. Sayers, *Hydraulic and Compressible Flow Turbomachines*. New York: McGraw-Hill, 1990.

[6] F. M. White *et al.*, *Fluid Mechanics*. New York: McGraw-Hill, 1994.

[7] B. R. Munson, D. F. Young, and T. H. Okiishi, *Fundamentals of Fluid Mechanics*. New York: Wiley, 1994.

[8] D. Chisholm, *Two-Phase Flow in Pipelines and Heat Exchangers*. New York: George Godwin, 1983.

[9] D. S. Miller, *Internal Flow Systems*. Cranfield, U.K.: BHRA (Information Services), 1990.

[10] A. F. Mills, *Basic Heat and Mass Transfer*. Homewood, IL: Irwin, 1995.

[11] P. J. Strachan, F. P. Reynaud, and T. W. von Backström, "The hydrodynamic modeling of torque converters," *R & D J.*, vol. 8, no. 1, pp. 21–29, 1992.

[12] *Handbook of Electric Motors*, R. H. Engelmann and W. H. Middendorf, Eds., Marcel Dekker, New York, 1995.

[13] *Heat and Mass Transfer in Rotating Machinery*, D. E. Metzger and N. H. Afgan, Eds., Hemisphere, Washington, DC, 1984.

[14] W. Y. Wong, *Heat Transfer for Engineers*. White Plains, NY: Longman, 1977.

[15] J. M. Owen, "The effect of forced flow on heat transfer from a disc rotating near a stator," *Int. J. Heat Mass Transfer*, vol. 14, pp. 1135–1147, 1971.

[16] ——, "The Reynolds analogy applied to flow between a rotating and a stationary disc," *Int. J. Heat Mass Transfer*, vol. 14, pp. 451–460, 1971.

[17] ——, "An approximate solution for the flow between a rotating and a stationary disk," *ASME J. Turbomach.*, vol. 111, no. 4, pp. 323–332, 1989.

[18] J. M. Owen and R. H. Rogers, *Flow and Heat Transfer in Rotating-Disc Systems*. Baldock, U.K.: Research Studies, 1989, vol. 1.

[19] N. F. Lombard, "Design and evaluation of an ironless stator axial flux permanent magnet machine," M.Sc. thesis, Univ. Stellenbosch, Dept. Elect. Eng., Matieland, South Africa, 1997.

[20] R. Wang and M. J. Kamper, "Evaluation of eddy current losses in axial flux permanent magnet (AFPM) machine with an ironless stator," in *Proc. IEEE Ind. Appl. Soc. Conf. Rec.*, Pittsburgh, PA, 2002.

Rong-Jie Wang (M'00) received the M.Sc. (Eng.) degree from the University of Cape Town, Cape Town, South Africa, in 1998 and the Ph.D. (Eng.) degree from the University of Stellenbosch, Matieland, South Africa, in 2003.

Currently, he is a Postdoctoral Research Fellow in the Department of Electrical Engineering, University of Stellenbosch. His research area is on special electrical machines, design optimization of electrical machines using the finite element method, thermal modeling of electrical machines, and renewable energy systems.

Maarten J. Kamper (M'96) received the M.Sc. (Eng.) and Ph.D. (Eng.) degrees from the University of Stellenbosch, Matieland, South Africa, in 1987 and 1996, respectively.

Currently, he is a Professor in the Department of Electrical Engineering, University of Stellenbosch. He was a Researcher with the SA Transport Services and the SA Council for Scientific and Industrial Research (CSIR) for several years. He is a South African National Research Foundation (NRF)-supported scientist. His research area is on computer-aided design and control of reluctance synchronous, switched reluctance, and permanent-magnet machine drives.

Robert T. Dobson received the B.Sc. (Eng.) degree in mechanical engineering from the University of Witwatersrand, Johannesburg, South Africa, in 1969 and the M.Sc. (Eng.) degree in nuclear engineering from the University of Cape Town, Cape Town, South Africa, in 1970.

Currently, he is a Senior Lecturer at the University of Stellenbosch, Matieland, South Africa, where he has been since 1988. He worked in the South African industry for 17 years before joining the lecturing staff. His research interests include energy production using natural circulation thermosyphon loops and thermal management and control using heat pipes.